Journal of Statistical Physics, Vol. 17, No. 2, 1977

Adsorption Isotherms for Fluids with Strong Interparticle Repulsions

E. R. Smith[1,3] and J. W. Perram[2]

Received December 14, 1976

We derive adsorption isotherms for an adsorbate of hard-sphere particles with "sticky" interactions at any fluid density being adsorbed onto a plane, "sticky" surface. The theory is based on the Percus–Yevick theory for bulk fluids and explicitly includes the equilibrium between the adsorbed fluid and the bulk adsorbate. The theory predicts a surface condensation at low temperatures and low bulk densities in good agreement with surface condensations found in experimental studies of adsorption of gases onto graphite. An approximate law of corresponding states for these transitions is developed. At higher bulk densities and room temperatures, the adsorption isotherms can show a maximum, in accord with recent experimental work.

KEY WORDS: Surface phase transitions; adsorption isotherms; dense fluids.

1. INTRODUCTION

Recently we have developed a method for describing the microscopic structure of a dense fluid or dense fluid mixture (like a solution) in the vicinity of a plane adsorbing surface.[1–3] In the theory of bulk simple liquids it is known that the most important feature of the interparticle potential for determining the microscopic structure of the liquid is the repulsive core.[4] Further, the repulsive core may be replaced by a hard-sphere potential of appropriate diameter without changing the structure of the liquid.[5] In this paper we assume that the same principle holds true for adsorption phenomena. That

Supported by the Australian Research Grants Commission.

[1] Department of Applied Mathematics, University of Waterloo, Waterloo, Ontario, Canada.

[2] Department of Mathematics, University of Odense, Odense, Denmark.

[3] Permanent address: Department of Mathematics, University of Melbourne, Parkville, Victoria, Australia.

is, the repulsive core of the interparticle potential is the main determinant of the adsorbate structure and a model system with an appropriate hard-sphere potential will give an accurate description of that structure.

To describe the adsorption of a mixture of M species of hard spheres (with densities ρ_α and diameters R_α, $\alpha = 1,..., M$) onto a plane surface, we first consider a bulk system of $M + 1$ different species. In this bulk system we write the probability for finding a particle of species α within $d^3\mathbf{r}_1$ of $\mathbf{r}_1$ and a particle of species β within $d^3\mathbf{r}_2$ of $\mathbf{r}_2$ as

$$n_{\alpha,\beta}(\mathbf{r}_1, \mathbf{r}_2)\, d^3\mathbf{r}_1\, d^3\mathbf{r}_2$$

For an infinite system in which all potentials are spherically symmetric, the function $n_{\alpha\beta}$ depends only on $|\mathbf{r}_1 - \mathbf{r}_2|$. We now introduce the correlation functions g and h by the definitions

$$\int_{|\mathbf{r}|=r} n_{\alpha\beta}(|\mathbf{r}|)\, d^3\mathbf{r} = 4\pi r^2 \rho_\alpha \rho_\beta g_{\alpha\beta}(r)\, dr = 4\pi r^2 \rho_\alpha \rho_\beta [h_{\alpha\beta}(r) + 1]\, dr \qquad (1)$$

The function $g_{\alpha\beta}$ has the properties

$$\lim_{r\to\infty} g_{\alpha\beta}(r) = 1$$

and

$$g_{\alpha\beta}(r) = 1 \qquad \text{for all } r \text{ for the ideal gas}$$

Thus $h_{\alpha\beta}$ is a measure of the departure of a system from ideality. We now consider the environment of an $M + 1$ species particle. We calculate the density of α species particles at a distance r from the surface of closest approach of an α particle to an $M + 1$ particle. This density is

$$\rho_\alpha [h_{M+1,\alpha}(R_{M+1,\alpha} + r) + 1]$$

where we define $R_{\alpha,\beta} = (R_\alpha + R_\beta)/2$. If we multiply this by the surface area of a sphere of radius $R_{M+1,\alpha} + r$ and divide by the area of the $(M + 1, \alpha)$ sphere of closest approach, we find the number of α particles at distance r from the $(M + 1, \alpha)$ sphere surface per unit area of $(M + 1, \alpha)$ sphere surface, and write this quantity

$$d_\alpha^*(r) = 4\pi(R_{M+1,\alpha} + r)^2 \rho_\alpha [h_{M+1,\alpha}(r) + 1]/4\pi R_{M+1,\alpha}^2 \qquad (2)$$

To study adsorption processes, we now take two limits on $d_\alpha^*(r)$. First we take the limit $\rho_{M+1} \to 0$, so that $d_\alpha^*(r)$ refers to the density of α particles about an *isolated* $M + 1$ species particle. We then take the limit $R_{M+1} \to \infty$, so that the surface of the isolated $M + 1$ species particle becomes planar and $d_\alpha^*(r)$ is the density per unit area of plane surface of α species particles a distance r from the plane surface. We write this density as

$$d_\alpha(r) = \lim_{R_{M+1}\to\infty} \lim_{\rho_{M+1}\to 0} d_\alpha^*(r) \qquad (3)$$

We note that it is essential to take the limits in the order shown.

To use Eqs. (2) and (3) it is necessary to have some characterization of the correlation functions $h_{\alpha\beta}$ to take limits with. To do this we first define, for the $M + 1$ species mixture, the direct correlation functions $C_{\alpha\beta}$ as the solutions of the Ornstein–Zernike relation[6–8]

$$h_{\alpha\beta}(r) = c_{\alpha\beta}(r) + \sum_{\gamma=1}^{M+1} \rho_\gamma \int d^3\mathbf{s}\, c_{\alpha\gamma}(|\mathbf{s}|)h_{\gamma\beta}(|\mathbf{r} - \mathbf{s}|) \tag{4}$$

This definition introduces a second set of functions $\{c_{\alpha\beta}\}$ about which we know little. To be able to evaluate $h_{\alpha\beta}$ and $c_{\alpha\beta}$ we must have a second relation between them. There is no known exact relation, but an approximate one which gives very good agreement with simulation studies for systems with strong repulsive cores to the interparticle potentials[9] is the Percus–Yevick approximation[10]

$$c_{\alpha,\beta}(r) = [1 - e^{\phi_{\alpha\beta}(r)/kT}][1 + h_{\alpha\beta}(r)] \tag{5}$$

where $\phi_{\alpha\beta}(r)$ is the interparticle potential. In this paper we calculate the correlation functions $h_{\alpha\beta}$ using Eqs. (4) and (5).

Taking the limits in Eq. (3) is much easier if we can solve Eqs. (4) and (5) analytically. To this end we introduce the potential

$$\exp[-(1/kT)\phi_{\alpha\beta}(r)] = \begin{cases} [R_{\alpha\beta}/12\tau_{\alpha\beta}(T)]\ \delta(r - R_{\alpha\beta} -), & r \leqslant R_{\alpha\beta} \\ 1, & r > R_{\alpha\beta} \end{cases} \tag{6}$$

with $\delta(x)$ the Dirac delta function. The parameters $\tau_{\alpha\beta}(T)$ are chosen so that the second virial coefficient for this potential is the same as that for some more realistic potential. The second virial coefficient is particularly easy to evaluate for this potential and we find

$$\tau_{\alpha\beta}(T) = R_{\alpha\beta}^3\left(1 + 3\int_0^\infty r^2\{\exp[-\phi_{\alpha\beta}^*(r)/kT] - 1\}\, dr\right)^{-1} \tag{7}$$

where $\phi_{\alpha\beta}^*(r)$ is some realistic interparticle potential. In this paper we use a Lennard-Jones potential throughout. The solution of the Percus–Yevick approximation for the sticky sphere mixture system has been calculated recently[11,12] and we use that solution. We note that several other workers have subsequently used the double limit procedure outlined above to study adsorption with other adsorption potentials.[13–15]

In Ref. 3 we developed this adsorption theory for adsorbates with only hard-sphere interactions between the adsorbate particles and a sticky adsorption potential. The structure of dense fluid adsorbates against a plane adsorbing surface shows large density oscillations as a function of distance from the surface. The wavelength of the oscillations for a one-component adsorbate is the particle diameter. Outside the first monolayer, the structure

of a strongly adsorbed dilute solute in a dense solvent is almost entirely determined by the solvent structure. Unfortunately, we can find at present no experimental results which confirm this picture. Thus it is of some interest to examine the adsorption isotherms from our sticky adsorption model to see how well they agree with experimental adsorption isotherms.

One set of isotherms of particular interest are those for the adsorption of gases onto exfoliated graphite and graphitized carbon.[16–19] The experimental adsorbing surfaces are highly planar [20] and the adsorbate particles are either spherical (krypton and xenon) or roughly spherical (methane). At low to intermediate monolayer coverage the isotherms show a sharp jump at temperatures in the range 50–100 K and at higher temperatures in this range they show a region of very rapid increase. Further, in the temperature range considered the adsorbing potential of graphite for these gases has a low minimum (12–15 kT) and very high curvature at the potential minimum (~ 500 kT nm^{-2}), so that the delta-function model for the adsorbing potential is not as bad as might be expected. The sharp jump in the adsorption isotherm is identified as a surface condensation from a dilute phase (possibly disordered gas) to a dense phase (possibly disordered liquid). From the point of view of verifying our model of adsorption from dense fluids, these transitions occur at unfortunately low bulk densities ($\eta_\alpha = \frac{1}{6}\pi\rho_\alpha R_\alpha^3 \approx 10^{-8}$), so that agreement between our model and experiment will not help in determining the accuracy of the model for dense adsorbates.

Another set of adsorption isotherms of interest are those measured by Ozawa *et al.*[21] for dense gases onto a molecular sieving carbon. The isotherms are measured at temperatures in the range -20°C to 60 °C and plotted as a function of bulk adsorbate fugacity from zero to about 100 atm. For the gases argon, nitrogen, carbon dioxide, and methane, these isotherms have a distinct local maximum. Other workers have also reported maxima in adsorption isotherms at high bulk adsorbate densities.[22,23] The isotherms measure the Gibbs surface excess density, which in our model would be

$$n_\alpha = \int_0^\infty [d_\alpha(x) - \rho_\alpha]\, dx \tag{8}$$

The maximum occurs because the region of space in which particles may be "adsorbed" eventually fills as ρ_α increases. When this region saturates, further increase of ρ_α means that n_α must decrease. The maximum appears to be a real effect of the hard-core repulsions between adsorbate particles. It occurs at relatively high densities for most adsorption studies ($\eta_\alpha = 0.05$–0.1) and thus is of interest to us in testing our adsorption model.

In this paper we give an outline of the solution of Eqs. (4) and (5) with potential (6) in Section 2. In Section 3 we develop expressions for adsorption isotherms using the two limits in Eq. (3). We find both the surface excess

[cf. Eq. (8)] and the adsorbed monolayer density. In Section 4 we apply this theory to the surface condensations discussed above, and find good agreement with experiment. We also develop an approximate law of corresponding states for adsorbed monolayer, dilute dense phase condensations. In Section 5 we apply the theory to the adsorption isotherm maxima discussed above and again find agreement with experimental results. We conclude the paper with a short discussion section.

2. THE STICKY (M + 1)-COMPONENT HARD-SPHERE MIXTURE

We solve the Percus–Yevick approximation for this system [Eqs. (4) and (5)] using Baxter's Wiener–Hopf factorization technique.[11,12] After Fourier-transforming, the Ornstein–Zernike relation (4) may be written in matrix form as

$$[I - \hat{C}(k)][I + \hat{H}(k)] = I \tag{8'}$$

where I is the $(M + 1) \times (M + 1)$ identity matrix and $\hat{H}_{\alpha\beta}$ and $\hat{C}_{\alpha\beta}$ are the Fourier transforms of $(\rho_\alpha\beta_\alpha)^{1/2}h_{\alpha\beta}(r)$ and $(\rho_\alpha\rho_\beta)^{1/2}c_{\alpha\beta}(r)$. The basis of Baxter's method is to write

$$I - \hat{C}(k) = \hat{Q}^T(-k)\hat{Q}(k) \tag{9}$$

where

$$\hat{Q}_{\alpha\beta}(k) = \delta_{\alpha\beta} - 2\pi(\rho_\alpha\rho_\beta)^{1/2}\int_{S_{\alpha,\beta}}^{R_{\alpha,\beta}} dr\, e^{ikr}q_{\alpha,\beta}(r) \tag{10}$$

with $S_{\alpha,\beta} = \frac{1}{2}(R_\alpha - R_\beta)$. The Percus–Yevick equation (5) enters because for the potential (6) we have

$$c_{\alpha\beta}(r) = 0 \qquad \text{for} \quad r > R_{\alpha\beta} \tag{11}$$

and this has the effect of restricting $q_{\alpha\beta}(r)$ to be nonzero only on $S_{\alpha,\beta} < r < R_{\alpha,\beta}$. Substitution of (9) and (10) into (8') and inversion of the Fourier transform[24,11] gives rise to

$$rh_{\alpha\beta}(r) = -q'_{\alpha\beta}(r) + 2\pi\sum_{\gamma=1}^{M+1}\rho_\gamma\int_{S_{\alpha,\gamma}}^{R_{\alpha,\gamma}} dt\, q_{\alpha\gamma}(t)(r - t)h_{\gamma\beta}(|r - t|) \tag{12}$$

for $r > S_{\alpha,\beta}$. We note that if $S_{\alpha,\beta} < r < R_{\alpha,\beta}$ and $S_{\alpha,\beta} < t < R_{\alpha,\beta}$, then $S_{\alpha,\beta} < |r - t| < R_{\alpha,\beta}$. For hard spheres we may write $h_{\alpha\beta}(|r|) = -1$ for $S_{\alpha,\beta} < r < R_{\alpha,\beta}$ and for this range of r replace $h_{\alpha\beta}(r)$ by -1 both on the left side of Eq. (12) and in the integrand of Eq. (12). This shows that $q'_{\alpha\beta}(r)$ is linear and $q_{\alpha\beta}(r)$ quadratic on that range. If we look at the first term in the

graphical expansion of $h_{\alpha\beta}(r)$ (the o—o term), we see that it is sensible to suggest the form

$$h_{\alpha\beta}(r) = -1 + \tfrac{1}{12}\lambda_{\alpha,\beta}R_{\alpha,\beta}\delta(r - R_{\alpha\beta} -) \qquad \text{for} \quad S_{\alpha,\beta} < r < R_{\alpha,\beta} \tag{13}$$

where the $\{\lambda_{\alpha\beta}\}$ are a set of numbers to be determined later. Since $q_{\alpha\beta}(r) = 0$ for $r > R_{\alpha\beta}$, Eq. (13) gives the discontinuity in $q_{\alpha\beta}(r)$ at $r = R_{\alpha\beta}$. We find

$$q_{\alpha\beta}(r) = \tfrac{1}{2}a_\alpha(r^2 - R_{\alpha\beta}^2) + b_\alpha(r - R_{\alpha\beta}) + \tfrac{1}{12}\lambda_{\alpha\beta}R_{\alpha\beta}^2 \tag{14}$$

where

$$a_\alpha = (1 - \xi_3 + 3R_\alpha\xi_2)/(1 - \xi_3)^2 - X_\alpha/(1 - \xi_3)$$

$$b_\alpha = -3R_\alpha{}^2\xi_2/2(1 - \xi_3)^2 + R_\alpha X_\alpha/2(1 - \xi_3)$$

$$\xi_j = \frac{\pi}{6}\sum_{\gamma=1}^{M+1}\rho_\gamma R_\gamma{}^j, \qquad X_\alpha = \frac{\pi}{6}\sum_{\gamma=1}^{M+1}\rho_\gamma\lambda_{\alpha\gamma}R_{\alpha\gamma}^2R_\gamma$$

If we insert (13) into (12), we can get an estimate of $\lambda_{\alpha\beta}$. Similarly, using the Fourier inverse of Eq. (9), we can calculate the amplitude of the delta function in $c_{\alpha\beta}(r)$ at $R_{\alpha\beta}$. If we insert the two calculations into the Percus–Yevick approximation, we obtain the set of coupled quadratic equations

$$\lambda_{\alpha,\beta}\tau_{\alpha,\beta} = a_\alpha + \frac{b_\alpha}{R_{\alpha\beta}} + \frac{\pi}{6}\sum_{\gamma=1}^{M+1}\rho_\gamma\frac{\lambda_{\beta\gamma}R_{\beta\gamma}^2}{R_{\alpha,\beta}}q_{\alpha\gamma}(S_{\alpha\gamma}) \tag{15}$$

The solution of these equations gives the set of numbers $\{\lambda_{\alpha\beta}\}$ and thus the functions $q_{\alpha\beta}(r)$. Numerical solution of Eq. (12) then gives the functions $h_{\alpha\beta}(r)$ for $r > R_{\alpha\beta}$. The structure of Eq. (12) allows its solution for $h_{\alpha\beta}(r)$ to proceed extremely quickly.[3,25]

3. ADSORPTION LIMIT OF THE STICKY MIXTURE

The methods necessary for taking the limits $\rho_{M+1} \to 0$ and then $R_{M+1} \to \infty$ on the above solution have been discussed carefully in an earlier paper,[3] so we do not discuss them in great detail here. We require the surface excess and monolayer adsorption isotherms. From Eq. (2) the surface excess is the double limit (3) of

$$n_\alpha{}^* = \rho_\alpha R_{M+1,\alpha}^2\int_0^\infty r^2h_{M+1,\alpha}(r)\,dr + \tfrac{1}{3}\rho_\alpha R_{M+1,\alpha} \tag{16}$$

Since the integral in this equation is the Fourier transform of $h_{M+1,\alpha}(r)$ at zero wave vector, we find, by substituting (9) into (8′), that

$$n_\alpha{}^* = \frac{1}{3}\rho_\alpha R_{M+1,\alpha} + \left(\frac{\rho_\alpha}{\rho_{M+1}}\right)^{1/2}\frac{\{[\hat{Q}(0)]^{-1}[\hat{Q}^T(0)]^{-1} - I\}_{\alpha,M+1}}{4\pi R_{M+1,\alpha}^2} \tag{17}$$

It can be seen that various parts of this expression will diverge as $\rho_{M+1} \to 0$ and then $R_{M+1} \to \infty$. Extreme care must be taken to ensure that these divergenes cancel with other terms which are not so obvious in Eq. (17). The monolayer adsorption isotherm

$$m_\alpha = \lim_{R_{M+1}\to\infty} \lim_{\rho_{M+1}\to 0} \rho_\alpha \lambda_{M+1,\alpha} R_{M+1,\alpha}/12 \tag{18}$$

may be calculated more simply. We use it to study phase transitions in layers adsorbed from dilute gases. For the study of maxima in adsorption isotherms we naturally concentrate on the surface excess. From this point on we consider one-component adsorbates only, since we intend to examine experiments on one-component adsorbates, and much of the algebra gets out of hand with many components.

If we take the limit $\rho_2 \to 0$ and then $R_2 \to \infty$, Eqs. (15) reduce to

$$\tfrac{1}{12}\eta\lambda_{11}^2 - [\tau_{11} + \eta/(1-\eta)]\lambda_{11} + (1 + \tfrac{1}{2}\eta)/(1-\eta)^2 = 0 \tag{19}$$

and

$$L_{12}\left[T_{12} + \frac{\eta}{2(1-\eta)} - \frac{\lambda_{11}\eta}{12}\right] = \frac{1 + 2\eta - \eta(1-\eta)\lambda_{11}}{(1-\eta)^2} \tag{20}$$

where

$$\eta = \tfrac{1}{6}\pi\rho_1 R_1^3, \qquad L_{12} = \lim_{R_2\to\infty} R_{12}\lambda_{12}/R_1, \qquad T_{12} = \lim_{R_2\to\infty} \tau_{12}R_1/R_{12} \tag{21}$$

The monolayer adsorption isotherm is then given by

$$m_1 = (\rho_1 R_1/12)L_{12} \tag{22}$$

The parameter T_{12} is defined from Eq. (7). We obtain

$$T_{12} = \frac{R_1}{12}\left(\int_0^\infty \left\{\exp\left[-\frac{1}{kT}\psi(x)\right] - 1\right\} dx\right)^{-1} \tag{23}$$

The integral in Eq. (23) is simply the Henry's law coefficient [20] for an adsorption potential $\psi(x)$ onto a plane surface. Using Eq. (20), the monolayer adsorption isotherm becomes

$$m = \frac{\rho_1 R_1}{12(1-\eta)^2} \frac{1 + 2\eta - \eta(1-\eta)\lambda_{11}}{T_{12} + [\eta/2(1-\eta)] - \lambda_{11}\eta/12} \tag{24}$$

The calculation of the surface excess by taking limits of Eq. (17) is a little more complicated. The calculation goes through in exactly the same way as when $\lambda_{11} = 0$ (the case described in our earlier paper[3]) and so we do not repeat the details. A fairly tedious piece of algebra gives

$$n_1 = \frac{1}{6}\rho_1 R_1\left\{3 + \frac{\frac{1}{2}L_{12} - 3/(1-\eta)}{1 + \eta\{[(4-\eta)/(1-\eta)^2] - [\lambda/(1-\eta)]\}}\right\} \tag{25}$$

Equations (24) and (25) provide us with adsorption isotherms for the adsorbed monolayer density and the surface excess. In our discussion of experimental adsorption isotherms we use these expressions.

4. SURFACE TRANSITIONS AT VERY LOW BULK DENSITY

In experimental studies of the adsorption of noble gases onto graphite, adsorption isotherms rather like those sketched in Fig. 1 are seen,[16–18] and recent Monte Carlo simulation studies[19] of the adsorption of krypton onto graphite show similar isotherms. The feature of these isotherms that we wish to discuss is that as the bulk density (or pressure) increases at fixed temperature, the isotherm goes through a sudden, rapid increase, which is identified as a surface condensation transition at the lower temperatures. Above a "critical" temperature, the increase is of finite gradient but is still very steep. In this section we calculate the bulk density for the transition as a function of temperature and compare this with the experimental bulk density at which the surface is 40% covered (the critical surface density identified by Thomy and Duval[16]).

The horizontal axis in Fig. 1 shows these transitions occurring at bulk pressures of 10^{-3} Torr, low enough to use the ideal gas law to determine the bulk density from the bulk pressure. The density at which the transitions occur is $\eta \approx 10^{-8}$–10^{-7}. (We discuss the choice of hard-sphere diameter for

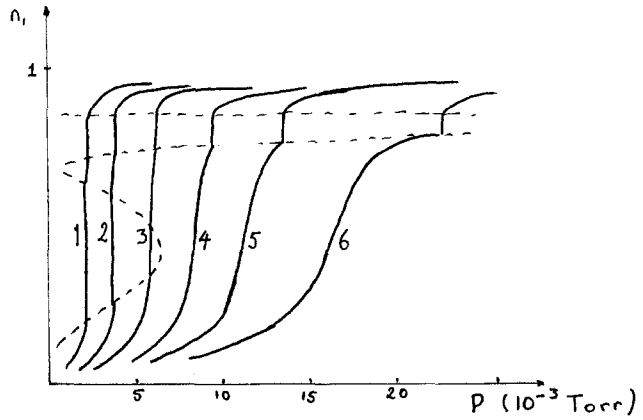

Fig. 1. Sketch of adsorption isotherms of krypton on graphitized carbon expressed as a fraction of monolayer coverage by krypton at 77.3 K. (1) 82.4 K; (2) 84.1 K; (3) 85.7 K; (4) 87.1 K; (5) 88.3 K; (6) 90.1 K.

the gas particles below.) At such small values of η we may expand the surface excess in powers of η to find

$$n_1 = (\rho_1 R_1/12)L_{12}[1 + O(\eta)] = m[1 + O(\eta)] \tag{26}$$

so that in this section we consider the simpler monolayer density of Eq. (24) as a measure of the amount adsorbed.

If we examine Eq. (24), we see that it may have a simple pole at a finite positive density, because the denominator becomes zero. On the high-density side the monolayer density is negative, which is physical nonsense. However, on the low-density side the monolayer density increases until it diverges at same value $\eta(T)$. We identify this divergence as the limit of metastability of the low-density surface phase. The sticky gas model in the Percus–Yevick approximation cannot connect the bulk liquid and bulk gas phases in a two-phase region: The answers come out in complex numbers. In the same way it cannot connect the dense surface phase with the dilute bulk and surface phases—a range of negative surface densities results. It can, however, connect the dilute bulk and surface phases and thus predict the condensation. We note that the denominator of Eq. (24) is still negative when the bulk system undergoes a transition to a liquid state, but the numerator changes sign on the liquid side of the spinodal curve, so that for the liquid state the adsorbed monolayer density is positive. At temperatures above the critical temperature of the bulk, these problems do not arise in the same way.

If we insert the solution of Eq. (19) into (24) we see that the divergence occurs when η is the solution of

$$2T_{12} - \tau_{11} = -\{[\tau_{11} + \eta/(1 - \eta)]^2 - \tfrac{1}{3}\eta(1 + \eta/2)/(1 - \eta)^2\}^{1/2} \tag{27}$$

From Eq. (7) we see that τ_{11} is a measure of the strength of the adsorbate–adsorbate attractions. For weak enough attractions ($\tau_{11} < 2T_{12}$) there is no condensation. To evaluate τ_{11} we use a Lennard-Jones potential

$$\phi_{11}^*(r) = 4\epsilon[(\sigma/r)^{12} - (\sigma/r)^6] \tag{28}$$

The hard-sphere diameter is taken to be σ. To evaluate T_{12} via Eq. (23) for gas particles interacting with a graphite surface, we use the potential introduced by Steele[20] and used in Monte Carlo simulations of adsorption processes by Lane and Spurling.[19] The potential for a gas α is

$$\psi_\alpha(x) = 2\pi q\epsilon(\alpha, C)[\sigma(\alpha, C)]^2\left\{\frac{2}{5}\left[\frac{\sigma(\alpha, C)}{x}\right]^{10} - \left[\frac{\sigma(\alpha, C)}{x}\right]^4 - \frac{[\sigma(\alpha, C)]^4}{3\Delta x(x + 0.61\,\Delta x)^3}\right\} \tag{29}$$

Table I. Lennard-Jones Parameters Used in the Calculations

	ϵ/k, K	σ, nm
Krypton[26]	168.8	0.367
Xenon[27]	221.0	0.4100
Methane[27]	148.2	0.3817
Carbon[19]	27.0	0.345

In Eq. (29) the parameters $\sigma(\alpha, C)$ and $\epsilon(\alpha, C)$ are those for the α molecule–carbon atom Lennard-Jones potential determined from the Lorentz–Berthelot combining rules:

$$\sigma(\alpha, C) = \tfrac{1}{2}[\sigma(\alpha, \alpha) + \sigma(C, C)], \qquad \epsilon(\alpha, C) = [\epsilon(\alpha, \alpha)\epsilon(C, C)]^{1/2}$$

where $\sigma(\alpha, \alpha)$ and $\epsilon(\alpha, \alpha)$ are the parameters of Eq. (28) for the α–α interaction and $\sigma(C, C)$ and $\epsilon(C, C)$ are those for carbon atoms in graphite. The other symbols in Eq. (29) are: q, the number of carbon atoms per unit area in the basal plane of graphite (taken as 38.18 atom nm^{-2}) and Δx, the interlayer spacing in graphite (taken as 0.34 nm). We give a list of the Lennard-Jones potential parameters used in this paper in Table I.

In Fig. 2 we plot $\eta(T)$ as a function of absolute temperature for krypton and plot the experimental data of Thomy and Duval[16] and the three simulation points of Lane and Spurling.[19] The agreement between theory and experiment is good, but the data are at consistently lower densities than the theory. Two possible causes of this discrepancy are inaccurate pair potentials and the fact that a real condensation will always take place at lower density than its metastable limit. We note that we have plotted points beyond the

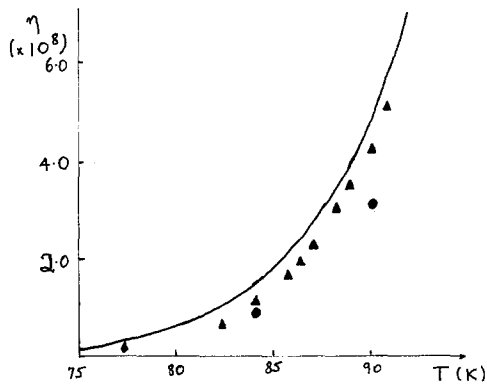

Fig. 2. (———) Plot of $\eta(T)$ from Eq. (27) for krypton. (▲) Data of Thomy and Duval[16] for 40% coverage. (●) Simulation data of Lane and Spurling.[19]

"critical temperature" for the transition found by Thomy and Duval and others.[16–18] The third point of the simulation data[19] also corresponds to a transition (jump in the adsorption isotherm) above the observed critical point. Certainly this is a region where the isotherm is increasing very rapidly and this is reflected in the divergence of m_1 at $\eta = \eta(T)$.

If we note that $\eta(T)$ is very small, we can construct an approximate law of corresponding states for the transition from an approximate solution of Eq. (27). We define the reduced temperature T^* for some fluid as

$$T^* = kT/\epsilon \tag{30}$$

where ϵ is the Lennard-Jones potential energy parameter for the fluid, and the reduced second virial coefficient by

$$B'(T^*) = B_2(\epsilon T^*/k)/2\pi R_1^3 \tag{31}$$

where R_1 is the Lennard-Jones potential distance parameter for the fluid and

$$B_2(T) = 4\pi \int_0^\infty r^2 \left(\exp\left\{ -\frac{4\epsilon}{kT} \left[\left(\frac{R}{r}\right)^{12} - \left(\frac{R}{r}\right)^6 \right] \right\} - 1 \right) dr \tag{32}$$

so that

$$B'(T^*) = 2 \int_0^\infty x^2 \{ \exp[-(4/T^*)(x^{-12} - x^{-6})] - 1 \}\, dx \tag{33}$$

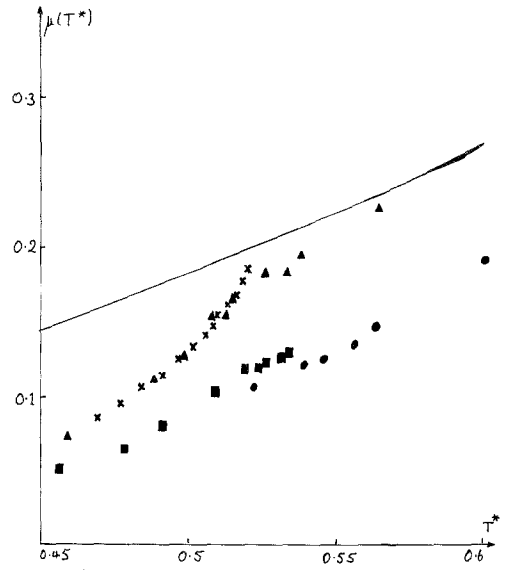

Fig. 3. (———) Plot of $\mu(T^*)$ from Eq. (34). Data of Thomy and Duval for krypton (▲), xenon (■), and methane (●). Data of Larher for krypton (×).

An approximate solution of (27) is then

$$\mu(T^*) \equiv 2\eta(\epsilon T^*/k)K(\epsilon T^*/k)/R = [3B'(T^*) - 1]^{-1} \tag{34}$$

which provides us with an approximate "universal curve" or "law of corresponding states" for the bulk adsorbate density at which the transition occurs. In Fig. 3 we plot $\mu(T^*)$ from Eq. (34) and some experimental data. The agreement is fair, but not so good for xenon and methane as for krypton. This may be because the potential parameters for krypton are more recent estimates[26] than those for methane and xenon.[27] The data for xenon and methane are those for a best fit of a second virial coefficient for a Lennard-Jones potential to experimental results. Since we use them in evaluating the Henry's law constant $K(T)$, we cannot expect them to fit reality as well as parameters chosen for best fit for a wider range of experimental data, as was the case for krypton.[26]

5. MAXIMA IN ADSORPTION ISOTHERMS FOR DENSE FLUIDS

Figure 4 is a sketch of the data of Ozawa *et al.*[21] for the adsorption of methane onto molecular sieving carbon. Recent studies have shown that at low pressures, adsorption isotherms for gases onto carbon do not vary greatly from one form of carbon to another[28] and we assume that this is still true for dense adsorbates. That is, we assume that the surface is a graphite surface and the adsorption potential is of the form given in Eq. (29), using the parameters from Table I. The resulting adsorption isotherms are shown in Figure 5. They show good qualitative agreement with experiment. Unfortunately the

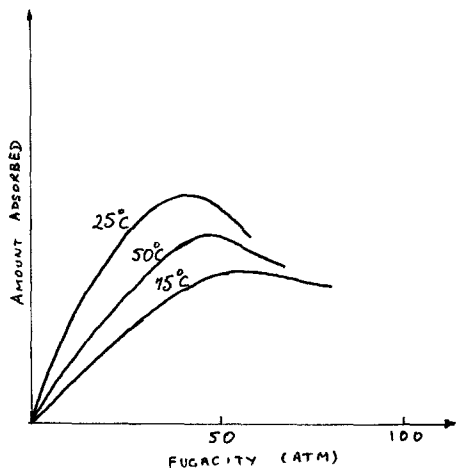

Fig. 4. Sketch of adsorption isotherms at high pressure for methane on millipore carbon sieves.[21]

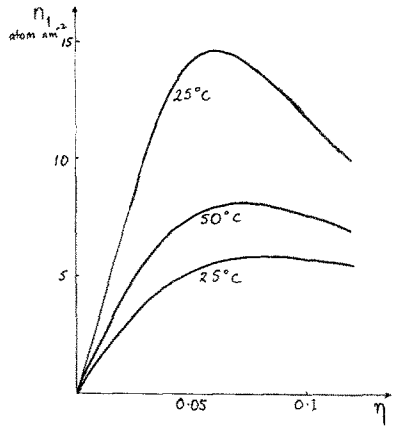

Fig. 5. Plot of surface excess n_1 in number adsorbed/nm^2, from Eq. (25) for methane on graphite.

data of Ozawa *et al.*[21] for the simple adsorption isotherm are not very accurately presented and so it is difficult to carry out a more detailed comparison. The maximum at ~ 14 atoms adsorbed per nm^2 at $T = 25°C$ corresponds to 2–3 close-packed monolayers on the surface.

Some very recent results of Specovius and Findenegg[29] on adsorption isotherms for argon on graphitized carbon also show a maximum. The maximum has been observed at $kT/\epsilon \sim 2.21$ and appears to shift to higher bulk densities and to widen as the temperature increases.

As noted in the introduction, the maxima in the adsorption isotherms occur because of the hard repulsions at close range between adsorbate particles. The qualitative agreement of our results suggest that our theory works well in accounting for repulsive interactions between adsorbate particles at high bulk adsorbate densities. We note that there is no pole in these adsorption isotherms because, as discussed above, the temperature is too high.

6. DISCUSSION

The agreement between our theory and experimental results for both low- and high-density fluid adsorbates suggests that our assumption of the importance of strong repulsive interactions in adsorption is essentially correct. A virtue of the theory is that it treats the adsorbing region as part of a bulk inhomogeneous system. There is no need to treat the equilibrium between the bulk adsorbate and the vicinity of the adsorbed phase as an equilibrium between separate regions or phases by thermodynamics, since the results come naturally from statistical mechanics. Unfortunately the description of the adsorbed material is fairly primitive. It was necessary to assume that the surface was structureless and the theory did not lead to a

description of the two-particle correlation functions in the adsorbed layer region.

A proper confirmation of our adsorption model would require measurements of adsorbate structure in dense adsorbates close to the adsorbing surface. Techniques for such measurements do not appear to be available at present. Other applications of our theory do exist, however. Adsorption isotherms for dense fluid mixtures plotted as a function of concentration show both maxima and minima.[22] We are extending our analysis of adsorption isotherms for dense fluids to the case of binary and ternary mixtures at present.

REFERENCES

1. J. W. Perram and L. White, *J. Chem. Soc. Faraday Div. General Disc.* **59**:29 (1976).
2. J. W. Perram and E. R. Smith, *Chem. Phys. Let.* **39**:328 (1976).
3. J. W. Perram and E. R. Smith, *Proc. Roy. Soc. A*, **353**:193 (1977).
4. H. C. Andersen, D. Chandler, and J. Weeks, *J. Chem. Phys.* **56**:3812 (1972).
5. J. Barker and D. Henderson, *J. Chem. Phys.* **47**:2856 (1967).
6. L. S. Ornstein and F. Zernike, *Proc. Acad. Sci. (Amsterdam)* **17**:793 (1914) [reprinted in *The Equilibrium Theory of Classical Fluids*, H. L. Frisch and J. L. Lebowitz, eds. (Benjamin, 1964].
7. G. Stell, in *The Equilibrium Theory of Classical Fluids*, H. L. Frisch and J. L. Lebowitz, eds. (Benjamin, 1964).
8. R. J. Baxter, in *Physical Chemistry: An Advanced Treatise, VIIIA*, D. Henderson, ed. (Academic Press, 1971).
9. D. Henderson and E. W. Grundke, *J. Chem. Phys.* **63**:601 (1975).
10. J. K. Percus and G. J. Yevick, *Phys. Rev.* **110**:1 (1958).
11. J. W. Perram and E. R. Smith, *Chem. Phys. Lett.* **35**:138 (1975).
12. S. Barboy, *Chem. Phys.* **11**:357 (1975).
13. D. Henderson, F. Abraham, and J. Barker, *Mol. Phys.* **31**:1291 (1976).
14. E. Waisman, D. Henderson, and J. L. Lebowitz, *J. Chem. Phys.*, in press.
15. G. Stell, *J. Stat. Phys.*, in press.
16. A. Thomy and X. Duval, *J. Chim. Phys. Phys. Chim. Biol.* **67**:1101 (1970).
17. Y. Larher, *J. Chem. Soc. Faraday I* **70**:320 (1974).
18. F. A. Putnam and T. Fort, *J. Phys. Chem.* **79**:459 (1975).
19. J. E. Lane and T. H. Spurling, *Aust. J. Chem.*, in press.
20. W. A. Steele, *Surf. Sci.* **36**:317 (1973).
21. S. Ozawa, S. Kusumi, and Y. Ogino, *J. Coll. Inst. Sci.* **56**:83 (1976).
22. S. Sircar and A. L. Myers, *Am. Inst. Chem. Eng. J.* **19**:159 (1973); C. Minka and A. L. Myers, *Am. Inst. Chem. Eng. J.* **19**:453 (1973).
23. H. B. Gilmer and R. Kobayashi, *Am. Inst. Chem. Eng. J.* **10**:797 (1964).
24. R. J. Baxter, *J. Chem. Phys.* **52**:4559 (1970).
25. J. W. Perram, *Mol. Phys.* **30**:1505 (1975).
26. C. Thomas, R. Van Steenwinkel, and W. Stone, *Mol. Phys.* **5**:301 (1962).
27. J. O. Hirschfelder, C. F. Curtis, and R. B. Bird, *Molecular Theory of Gases and Liquids* (Wiley, 1964).
28. M. Matecki, A. Thomy, and X. Duval, *Comp. Rend. Acad. Sci. C* **281**:639 (1975).
29. J. Specovius and G. H. Findenegg, to be published.